MAX-PLANCK-GESELLSCHAFT

Journal of Catalysis, 236 (2005), 324-334

Rapid Genesis of Active Phase during Calcination of Promoted Sulfated Zirconia Catalysts

A.H.P. Hahn, R.E. Jentoft, T. Ressler, G. Weinberg, R. Schlögl, F.C. Jentoft*

Department of Inorganic Chemistry, Fritz-Haber-Institute of the MPG, Faradayweg 4-6, 14195 Berlin, Germany

* Corresponding author: e-mail jentoft@fhi-berlin.mpg.de, , phone: +49 30 8413 4408, fax +49 30 8413 4693

Received 28 July 2005, Revised 27 September 2005, accepted 27 September 2005

Abstract

Amorphous sulfated zirconium hydroxide was promoted with iron or manganese via the incipient wetness technique, to give 0.5–3.5 weight% promoter in the final catalyst. An exothermic reaction during the calcination temperature ramp (to 823 or 923 K) leads to a rapid overheating ("glow") of the sample. XRD shows that crystallization starts before and progresses during the overheating. The surface area shrinks during the glow, and its final size (85–120 $m^2 \cdot g^{-1}$) and the porosity appear to be largely determined by the glow event. Manganese and iron ions prevent the coalescence of particles and lead to high surface areas. Variation of the batch volume (2.2, 8.4, or 17.1 ml) for calcination produced different catalysts from the same precursor. For both promoters, samples calcined in large batches exhibited the highest surface areas, interconnected mesopores (2.2–3.8 nm), and the highest maximum rate in *n*-butane isomerization (338 K, 1 kPa *n*-butane). Long term performance was independent of surface area and morphology. The concentration of the active sites depended on the calcination batch size, indicating that the active phase is formed in kinetically controlled reactions during the rapid overheating. The catalytic and textural properties of sulfated zirconia catalysts can be reproduced through controlling the batch size used for calcination.

Keywords: promoted sulfated zirconia, iron, manganese, preparation, calcination, butane isomerization, morphology, in situ XRD

1. Introduction

Sulfated zirconia catalysts [1]have attracted interest because they are capable of isomerizing light alkanes such as butane at room temperature, where branched alkanes are thermodynamically favored [2]. Many attempts have been made to correlate the catalytic performance of sulfated zirconia to any of its other properties. Because the product distribution obtained in the conversion of alkanes [3,4] suggests acid catalysis, acid sites were a focus. Superacidic sites were inferred from the Hammett indicator method [5] but could not be found by adsorbing other probe molecules [6,7]. Some correlations turned out to be not simple, e.g. the tetragonal zirconia phase was long believed necessary for an active material [8], but newer results show activity also for the monoclinic phase [9] and for sulfated zirconia consisting of a mesoporous framework with amorphous walls [10].

The complexity of the analytical problem increased when it was discovered that the activity of sulfated zirconia can be improved by 1–2 orders of magnitude through addition of first row transition metal cations [11]. Besides an ongoing debate as to which promoter is best [12,13], their exact function is even more controversial. Initially these promoters were believed to boost the acidity [14]but the evidence did not hold [15-17]. It has been proposed that a redox functionality is introduced with the promoters, and alkanes might be activated via oxidative dehydrogenation [18] but corresponding reduction of the promoter is not always detected [19-22]. In a recent publication [23] we demonstrated that iron or manganese cations are incorporated into the zirconia lattice and thus might act as structural promoters by stabilizing the tetragonal phase, and as electronic promoters through their lower valence in comparison to Zr(IV) and the defects that are generated in effect.

Establishing relationships between preparation parameters and material's properties or between structure and activity for sulfated zirconia catalysts has been hampered by two facts. 1) The reproducibility of the materials has so far been poor, e.g. Keogh et al. [24] found for different batches

of the same sulfated zirconia preparation an average hexadecane conversion of 76.2% and a lowest measured conversion of 30.2%. Reports on the state and dispersion of the promoters differ greatly for preparations of different laboratories [23 and references therein]. 2) Some important sample properties are interdependent, e.g. if the sulfate content is changed, surface area and phase composition will be affected.

A successful synthesis route for these catalysts starts from X-ray amorphous zirconium hydroxide, which is treated with sulfate-containing solutions (e.g. ammonium sulfate, sulfuric acid) and optionally with solutions containing promoter cations [2,11]. Thermal treatment at 773–973 K in air (calcination) is the last preparation step. Important catalyst properties like sulfur content, surface area, phase composition, and activity have been correlated to the applied maximum temperature [2,25,26]. However, already while the raw material is heated to the calcination temperature many processes occur, such as water loss, decomposition of precursor species (ammonium, nitrates), crystallization, and sintering. Differential thermal analysis profiles, e.g. for pure zirconium hydroxide, show a sharp exothermic peak at around 725 K [2,27]. This "glow phenomenon" is not unique to zirconia; it has been observed for hydroxides of iron, chromium, and titanium [28-31] and is of general importance for the preparation of many catalysts. Tatsumi et al. correlated the catalytic activity of sulfated zirconia for *n*-pentane isomerization with the exotherm profile [32]. In a previous communication [33], we monitored the exotherm during calcination on preparative scale. Differently sized batches (2.2, 8.4, or 17.1 ml) of the same precursor material generated and experienced a different overheating effect during the exothermic reaction phase. For promoted sulfated zirconia, the *n*-butane isomerization activity increased strongly with increasing batch size used for calcination.

In this paper, we extend the work presented in [33] and aim (i) to demonstrate that the reproducibility of sulfated zirconia catalysts can be improved by controlling batch size and shape during calcination, (ii) to understand the calcination chemistry, and (iii) to identify which properties are affected by variations of the batch size and how they relate to catalytic performance.

2. Experimental

Catalyst preparation and thermal treatment

Amorphous zirconium hydroxide (ZH) and amorphous sulfated zirconium hydroxide with 5–6 wt% SO_3 (SZH) from MEL Chemicals (both white in color) were used as starting materials. After pre-drying for 21 h at 383 K and cooling in a desiccator, SZH-batches of 10.9 g were promoted by dropwise addition of appropriate amounts of aqueous solutions of $Fe(NO_3)_3 \cdot 9H_2O$ or $Mn(NO_3)_2 \cdot 4H_2O$ (both Merck p.a.) under vigorous stirring (incipient wetness method) [12] followed by drying at room temperature, to give *x*FeSZH and *x*MnSZH (*x* = promoter content after calcination in wt% metal). After impregnation the powders were dried at room temperature because SEM-EDX measurements revealed that drying at 380 K causes segregation of promoters to crust-edges. To avoid up-scaling effects during this step, always 10.9 g SZH were impregnated; larger amounts were obtained through mixing the dried powders thoroughly, but gently. Each mixture, obtained usually in one day, constitutes a precursor and is distinguished from other preparations of the same composition by its precursor number. Calcination was carried out in quartz boats [33] sized 2.2, 8.4 and 17.1 ml for ca. 3.5, 12, and 26 g of promoted precursor material. The smaller boats had the shape of semi-cylinders; the large boat enclosed the sample to > 50%. Single boats were placed in a 29 mm i.d. quartz tube in a horizontally mounted tubular furnace (Heraeus RO 4/25) with PID control. The quartz tube was purged with 200 $ml \cdot min^{-1}$ synthetic air and the oven was heated at 3 $K \cdot min^{-1}$ to 923 K (ZH, SZH: 823 K), held for 3 h at 923 K, a temperature recommended for best activity of promoted sulfated zirconia [26], and then cooled to room temperature. Some samples were thermally treated in argon or pure oxygen (250 $ml \cdot min^{-1}$). To monitor the actual sample temperature during calcination, an additional thermocouple was placed in the center of the sample bed. Thin (0.5 mm o.d.) sheath thermocouples (Thermocoax) were used for fast response and to minimize heat-sink effects. Analysis of the gas phase at the exhaust side of the calcination tube was performed with a Balzers gas inlet system GES 010 and a Balzers Prisma 200 quadrupole mass spectrometer (MS). The promoter content after calcination in selected samples was verified with atomic absorption spectroscopy and found to match the desired values without any measurable effect of the calcination in differently sized batches. Samples were named after their precursor number and the batch size (small, medium, large) used for calcination, e.g. 2.0MnSZ-1-S means 2.0MnSZ from precursor preparation number one, calcined in the small boat.

X-ray diffraction (XRD)

For ex-situ XRD measurements a STOE STADI P diffractometer and Cu $K\alpha_1$ radiation were used. Samples were mixed 50:50 by weight with corundum as internal standard. Diffractograms were recorded in Debye-Scherrer geometry with a primary monochromator and a curved position-sensitive detector with an internal resolution of 0.03° 2θ. In-situ XRD measurements were conducted using a STOE Bragg-Brentano diffractometer equipped with a secondary monochromator (Cu Kα radiation) and a scintillation counter. The precursor was dispersed on the resistively heated stainless steel band of a Bühler HDK S1 high-temperature cell mounted on the goniometer of the diffractometer. The cell was purged with 50 $ml \cdot min^{-1}$ of 21% O_2 in He. The average heating rate was 2.2 $K \cdot min^{-1}$. Between 570 and 870 K, the sample was heated in 9 K steps with an 18 $K \cdot min^{-1}$ heating rate and 2.5 min isothermal periods between

heating steps. During the isothermal periods, diffractograms were measured from 30 to 30.72° 2Θ with a 0.06° step size and a 10 s integration time.

Catalysis experiments

Samples were tested unpressed, since mechanical treatment (pelletization) has been shown to affect structure and reactivity of the catalysts [34]. Five hundred mg of sample were supported on a porous frit in a 13 mm i.d. once-through downward plug-flow fixed-bed glass reactor. After 30 min of activation at 723 K in flowing dry nitrogen, isomerization of *n*-butane (Linde 3.5) was carried out at 338 K and atmospheric pressure. Using mass flow controllers, 80 ml·min^{-1} of 1% *n*-butane in nitrogen were fed to the reactor. Analysis was performed by on-line gas chromatography, using a Varian 3800 GC equipped with a Chrompack plot fused silica 60 m capillary column (0.32 mm i.d.) and flame ionization detection.

Scanning electron microscopy (SEM)

Scanning electron micrographs and energy dispersive X-ray analysis (EDX) data were recorded with acceleration voltages of 5 or 15 kV on a Hitachi S-4000 SEM with a field emission gun and EDAX DX4. The different acceleration voltages resulted in EDX information depths of about 250 nm or 600 nm. The analyzed area was ≈1.75 μm^2.

Surface area and porosity

Adsorption and desorption isotherms were acquired using a Micromeritics TriStar 3000 at 77 K with N_2 as adsorbate. The samples were outgassed under vacuum at 473 K for ≈24 h before starting the measurements. For some samples, the conditions were varied between 423–623 K and 0.5–28 h to ensure that outgassing was complete while sample integrity was preserved. Data were processed with TriStar 3000 V3.00 software.

3. Results

Thermal treatment

Fig. 1a shows the bed vs. oven set temperature for 0.5MnSZH-1-L, 0.5FeSZH-1-L, 2.0FeSZH-1-L, 2.0MnSZH-1-L, and 3.5MnSZH-1-L. Because, during most of the calcination, the sample is being heated by the oven, the sample temperature (center of bed) lagged the oven set temperature. Beginning at an oven temperature of ≈480 K, a negative deviation from the set heating rate was observed for all samples. The deviation from the linear ramp reached a maximum of ca. -60 K at an oven temperature of ≈580 K; the return to a nearly linear increase occurred at 600–650 K. Water signals (mass charge ratios = 17, 18) were detected by MS during this phase, indicating that volatilization of water as a heat-consuming process causes the temperature lag. The deviation from the ramp was most pronounced for samples with 0.5 wt% promoter, consistent with an increasing fraction of water with decreasing promoter content in the room-temperature dried precursors. The mass/charge ratios 12, 43, and 44 were observed during the extended temperature lag for all samples, indicating desorption of CO_2, and possibly decomposition and combustion of hydrocarbon contaminants.

For some samples, small peaks in the sample temperature were observed at the end of the broad endotherm, e.g. at 600 K oven set temperature for 2.0MnSZH-1-L and at 650 K for 0.5FeSZH-1-L (see arrows in Fig. 1a). 0.5MnSZ-1-L did not produce such a peak, suggesting the slight overheating is not caused by a temperature control problem but by an exothermic reaction. Coupled thermogravimetric and MS analysis of such samples in 21% O_2/He flow show that the exothermic formation of N_2 is a possible explanation for these peaks. Continuing to heat past 600–650 K, the actual sample temperature followed the linear rate for a while. In this phase of the calcination, mass/charge ratio 30 (NO) was observed, indicating nitrate decomposition.

Between 750 K and 900 K, a rapid overheating (glow phenomenon) was observed for all samples. The onset shifted to higher temperatures with increasing promoter content. Small Mn contents were without significant effect, e.g. 0.5MnSZH-1-L glowed beginning at 760 K, which is near the oven temperature at which SZH started to glow [see 33]. At promoter contents of 2 wt% and higher, the shift of the onset towards higher temperatures with increasing promoter content was more pronounced for Mn than for Fe. The measured overshoot approached values of up to 200 K for these samples calcined in large batches; the measured maximum temperature was ≈970 K. Heating rates reached values up to 1700 K·min^{-1}. Because the thermocouple is large in diameter in comparison to the particles (0.5 mm vs. 15 μm) and relative to the sample a good thermal conductor, actual heating rates and temperatures will be higher than those measured. The *m/q*-ratios of 48 and 64 for SO_2 were not detected during the whole calcination procedure.

Fig. 1b shows the bed temperature vs. oven set temperature of 2.0FeSZH-1 with the batch size as parameter. The onset temperature for the glow was lowest in the large batch, followed by the medium and the small batch. In most cases, calcinations in larger batches produced also larger glow peaks. The measured temperatures in the large batch (2.0FeSZH-1-L) during the glow exceeded the highest programmed oven temperature of 923 K. For 2 wt% Mn-promoted samples, the same trend was shown with variation of the batch size, but the glow onset temperatures were higher than those of the corresponding Fe-promoted samples [33]. A special behavior of the 2.0FeSZH samples is seen at an oven temperature of about 800 K: the profiles in the small and medium batch exhibit an ≈10 K step-increase of the sample temperature at ≈10 K before the beginning of the full

glow. This behavior was absent for samples with lower Fe-content or Mn-promotion. This effect is not observed in the large batch, presumably because it is overwhelmed by the earlier rapid temperature rise. Variations of the glow curves obtained for different precursors at equal batch size were smaller for Mn- than for Fe-promoted samples.

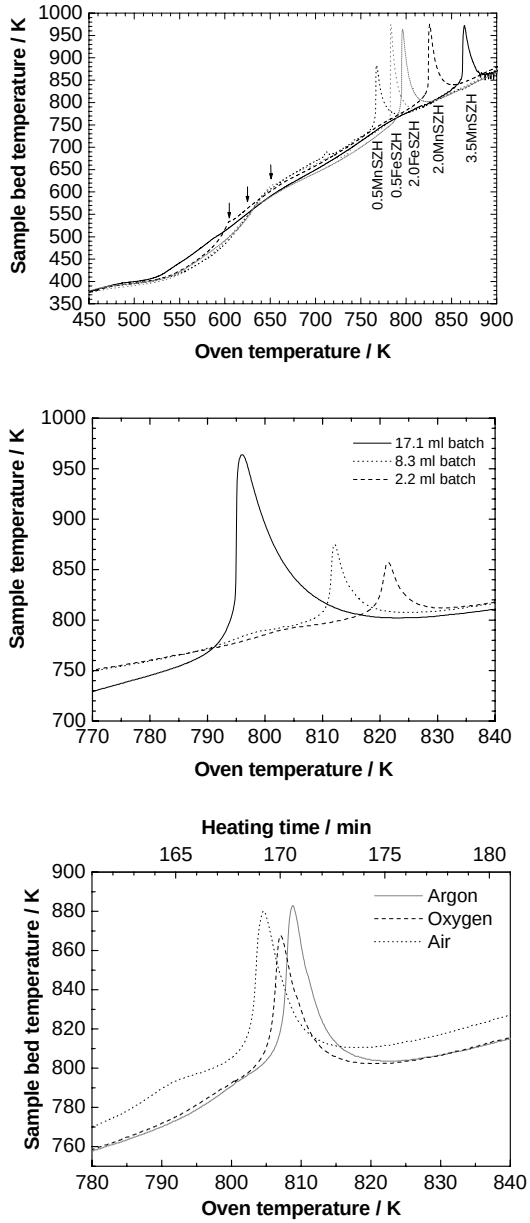

Figure 1: a) Sample bed temperature versus nominal oven temperature in 17.1 ml batches during thermal treatment of Mn and Fe-promoted samples; heating rate 3 K·min^{-1}, 200 ml·min^{-1} air flow. **b)** Sample bed temperature versus nominal oven temperature during thermal treatment of a 2 wt% Fe-promoted sample (2.0FeSZH-1) in differently sized batches with 2.2, 8.4 or 17.1 ml volume, heating rate 3 K·min^{-1}, 200 ml·min^{-1} air flow. **c)** Sample bed temperature versus nominal oven temperature during thermal treatment of 2 wt% Fe-promoted sample in an 8.4 ml batch, heating rate 3 K·min^{-1}, 200 ml·min^{-1} air flow (2.0FeSZH-2) or 250 ml·min^{-1} flow of Ar or O_2 (2.0FeSZH-3).

The effect of different atmospheres on the glow peak of 2.0FeSZH samples during thermal treatment in a medium-sized batch is presented in Fig. 1c. The onset-temperature varied by 5 K, but there was no correlation with the O_2 content or thermal conductivity of the gas in the group Ar, air, and O_2. The extent of the glow and the general shape also were not affected in a significant way.

The color of Fe-promoted samples changed during calcination from ochre to rust-colored, that of Mn-promoted samples from beige-pink to light bluish-gray or darker gray. The intensity of the colors increased with increasing promoter content.

Bulk structural changes during the glow

In order to identify the events during the glow the simplest system, i.e. zirconium hydroxide, was calcined in a medium batch to a set temperature of either 663 K or 713 K, held there for 1 min, and cooled with a 3 K·min^{-1} programmed ramp. The glow onset for this sample–batch size

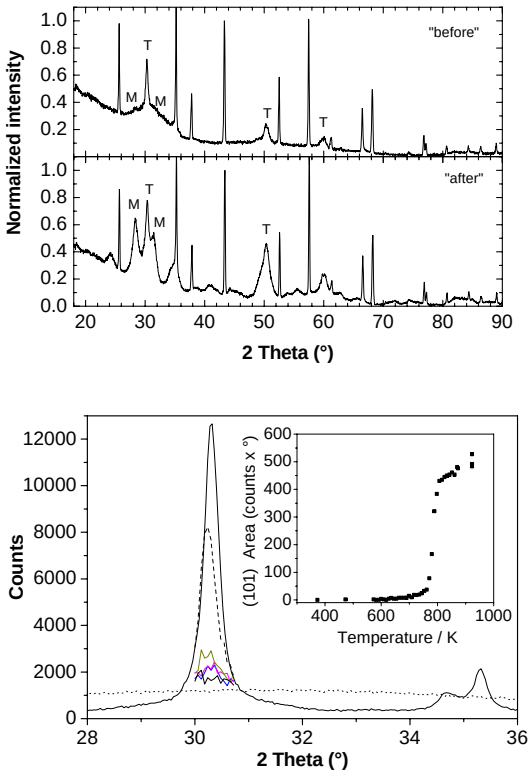

Figure 2: a) X-ray diffractograms of zirconium hydroxide previously calcined in an 8.4 ml batch with a holding time of 1 min at 663 K ("before" glow) or 713 K ("after" glow). Narrow reflections from internal standard α-Al_2O_3 (50:50 by weight). Intensity normalized to 2θ = 43.3° reflection of the standard. Main reflections of tetragonal (T) and monoclinic (M) phases indicated.**b)** X-ray diffractograms of 2 wt% Fe-promoted sample FeSZH-1 recorded in situ in a flow of 21% O_2 in He; heating rate 18 K·min^{-1} with isothermal periods during data acquisition (average rate 3 K·min^{-1}). Inset: area of (101) reflection vs. temperature.

combination is found at ≈690 K and hence, one sample underwent the glow (evidenced by the temperature measurement during calcination, denoted as "after"), while the other did not ("before"). Fig. 2a shows the corresponding X-ray diffractograms. To assess the fraction of non-crystalline material, an internal standard was added. The diffractogram of the sample "before" the glow shows, although ill-defined, reflections of both the tetragonal and the monoclinic phases. From comparison of the zirconia reflections in the "before" and "after" samples with internal standard reflections it becomes evident that conversion to the tetragonal and monoclinic phases progresses further during the glow. Significant was the reduction of the BET surface area of this sample from 244 $m^2 g^{-1}$ "before" to 122 $m^2 g^{-1}$ "after" the glow. Furthermore, pores generating an H2-type N_2 adsorption hysteresis develop during the glow.

In-situ XRD data obtained during the heating of FeSZH-1 are presented in Fig. 2b. The amount used for such an experiment is about 30 mg and is spread over an area of approximately 1 cm^2 on a stainless steel heating band. The most intense reflection (101) of the tetragonal phase becomes first discernable at about 730 K. The reflection begins to grow rapidly at about 760 K and by 810 K it reaches 89% of the maximum area, which is achieved at 923 K. The onset of crystallization is at a lower temperature than the sample temperature at the onset of the glow for all three batch sizes.

n-Butane isomerization

For a large number of samples with promoter contents of Fe or Mn in the range of 0.5–3.5 wt%, the *n*-butane isomerization activity increased with increasing calcination batch size. Independent of this trend, three different types of behavior can be distinguished.

Fig. 3a shows the 2.0FeSZ-1 set, together with 2.0FeSZ-2-L for determination of the reproducibility. All samples exhibited a fast increase in conversion, which reached almost 20% for the large-batch samples, followed by deactivation. After 8 h, the conversion level corresponded to ≈20% of the respective maximum activity. This long-term activity is approximately one order of magnitude higher than that of unpromoted sulfated zirconia.

In Fig. 3b, the conversion to isobutane with time on stream is plotted for the 2.0MnSZ-1 set and 2.0MnSZ-2-L. The conversion increased and declined more rapidly compared to the Fe-promoted samples, while the maximum conversion was similar. The remaining activity after 8 h corresponded to about 2% of the maximum conversion, and the rates are slightly higher, but in principle comparable to those obtainable with sulfated zirconia.

Fig. 3c shows the performance of the 0.5MnSZ-1 set. The conversion increased more slowly than for the samples with higher promoter content. The catalysts deactivated only gradually and at 8 h on stream, the conversion was still at ≈50% of the maximum conversion. The long-term activity (8 h) was comparable to those of the 2.0FeSZ set, or even higher.

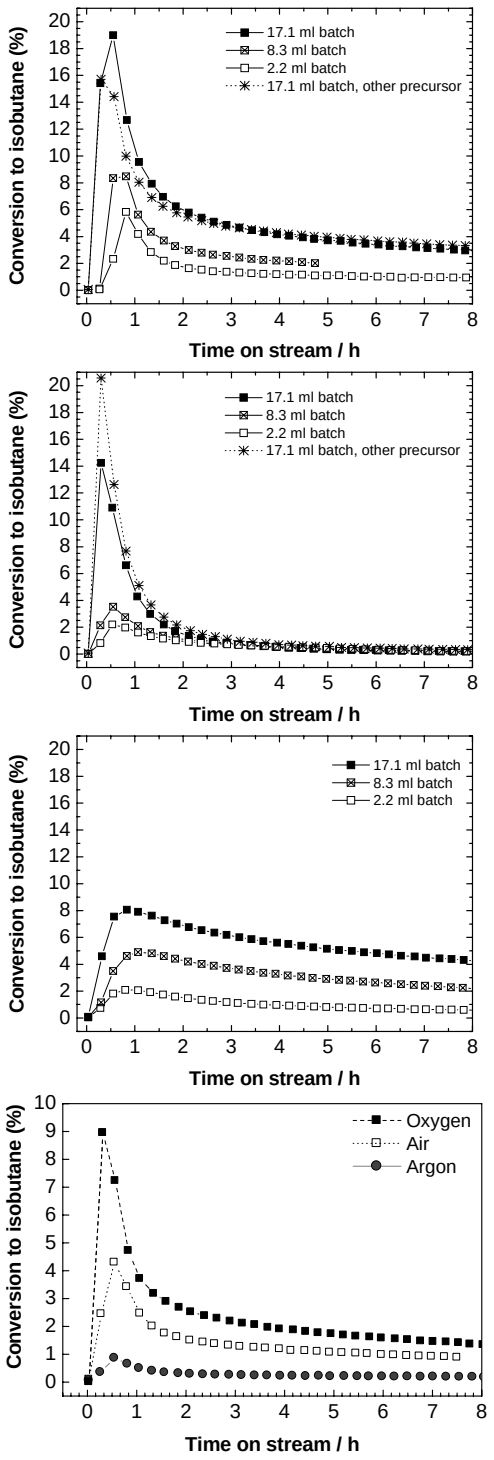

Figure 3: Conversion to isobutane vs. time on stream; 500 mg catalyst, reaction temperature 338 K, 1 kPa *n*-butane in N_2, total flow 80 ml·min^{-1}. **a)** 2 wt% Fe-promoted sulfated zirconia, calcination in differently sized batches, 2.0FeSZ-1 (squares) and 2.0FeSZ-2-L (stars). **b)** 2 wt% Mn-promoted sulfated zirconia, calcination in differently sized batches, 2.0MnSZ-1 (squares) and 2.0MnSZ-2-L (stars). **c)** 0.5 wt% Mn-promoted sulfated zirconia, calcination in differently sized batches, 0.5MnSZ-1. **d)** 2 wt% Fe-promoted sulfated zirconia, thermal treatment in different atmospheres, batch size 8.4 ml, 2.0FeSZ-3 (solid symbols) and 2.0FeSZ-2-L (open symbols).

In Fig. 3d, the performance of the 2.0FeSZ samples heat-treated in a medium size batch in different atmospheres is depicted. The maximum and also the long term isomerization rates show a clear trend O_2 > air > Ar.

Scanning electron microscopy

SEM micrographs of 2.0FeSZ-2 samples, calcined in large or small batches, reveal a particle size around 15 µm, equal to that of the sulfated zirconium hydroxide precursor. Roughness varied among different particles; the smallest

Figure 4a

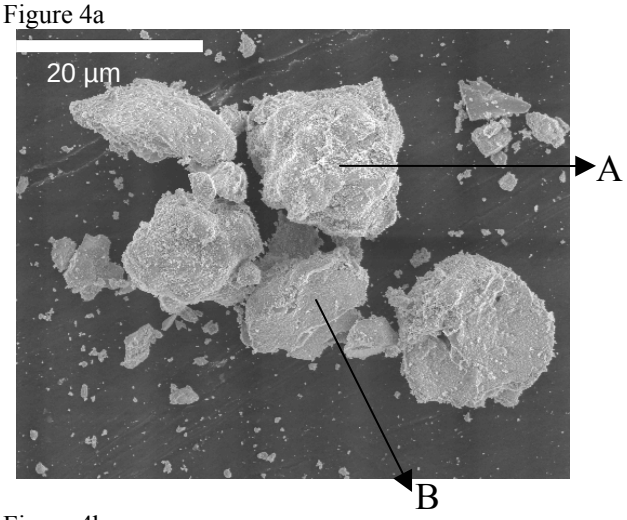

Figure 4b

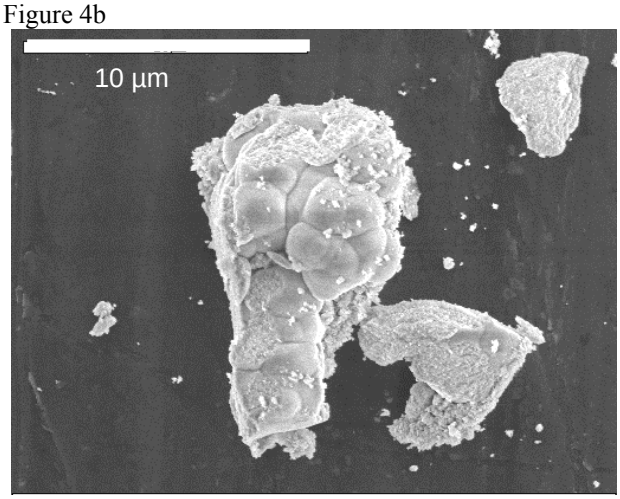

Figure 4: SEM images of **a)** 2 wt% Fe-promoted sulfated zirconia, calcined in 2.2 ml batch, 2.0FeSZ-2-S. **b)** 2 wt% Mn-promoted sulfated zirconia, calcined in 2.2 ml batch, 2.0MnSZ-1-S.

variations were observed in 2.0FeSZ-2-L. EDX measurements of 2.0FeSZ-2-S (Fig. 4a) at Point A (rough) gave ≈3.5 wt% Fe and a barely discernable S signal. Apparently, in rough areas Fe is enriched near the surface. No S signal could be detected at Point B (smooth), and only using the more deeply penetrating 15 keV electrons about 2 wt% Fe was detected. In catalytically inactive 2.0FeSZ samples (not shown here) Fe was always accompanied by S, suggesting that failed preparations had produced iron sulfate.

Table 1: BET surface areas, BET constants c, and BJH cumulative pore areas

Sample	BET surface area / m^2g^{-1}	BET constant c	BJH Adsorption cum. pore area* / m^2g^{-1}
2.0FeSZ-1-S	106	56	80
2.0FeSZ-1-M	112	54	100
2.0FeSZ-1-L	120	57	137
2.0FeSZ-2-L	113	72	125
2.0MnSZ-1-S	86	57	70
2.0MnSZ-1-M	89	56	72
2.0MnSZ-1-L	109	68	121
2.0MnSZ-2-L	117	56	137
0.5MnSZ-1-S	92	58	68
0.5MnSZ-1-M	96	72	112
0.5MnSZ-1-L	106	76	131

*calculated from adsorption branch after the BJH method [54] (calculation from desorption branch would lead to erroneous results with this type of hysteresis)

In addition to particles resembling those of the 2.0FeSZ-2 series, 0.5MnSZ-1 and 2.0MnSZ-1 samples contained slightly smaller particles with a smoother appearance, possibly because fewer fine particles adhere to their surfaces than in the Fe-promoted samples. For Mn-promoted samples calcined in a small batch, these smooth areas showed a substructure, indicating individual smaller particles of roundish shape and a size of 2–3 µm, see Fig. 4b. Neither Mn nor S could be detected using EDX.

Surface area and porosity

An overview of BET surface areas is given in Table 1. In general, surface areas increased with increasing calcination batch size, e.g. 86 to 109 $m^2 \cdot g^{-1}$ for the 2.0MnSZ series. Differences between Mn- and Fe-promoted samples with 2 wt% promoter content were slight for large batch calcinations; Mn-doped samples calcined in a medium or small batch tended to have a lower surface area than the corresponding Fe-containing samples.

Examples of nitrogen adsorption isotherms are shown in Fig. 5a (2.0FeSZ-1 series and of 2.0FeSZ-2-L) and Fig. 5b (0.5MnSZ-1). All isotherms can be classified as type IV, which implies mesoporosity. Isotherms of samples calcined in small batches expressed nearly no hysteresis loops, while those of samples from large batches showed H2-type loops. The isotherm shapes indicate a transition from open, wedge- or cone-shaped pores to a porous network of interconnected channels with different diameters [35] upon increase of

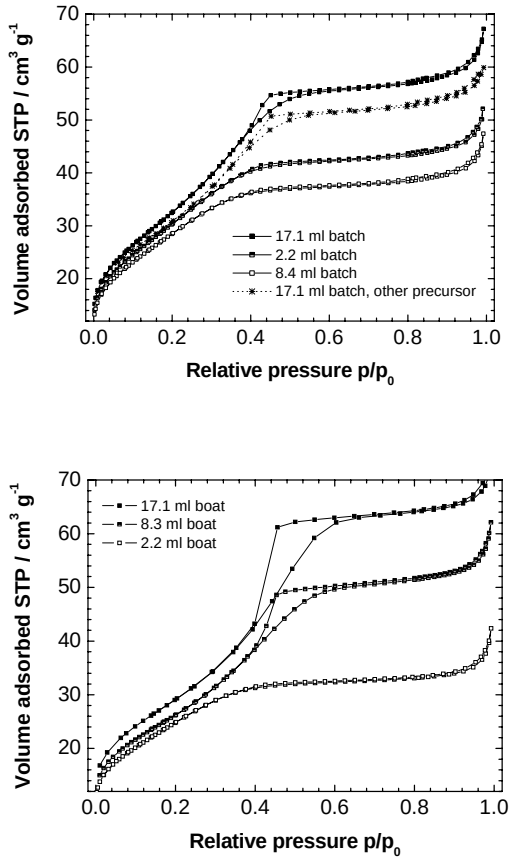

Figure 5: Adsorption and desorption branches of nitrogen adsorption isotherms at 77 K. **a)** 2 wt% Fe-promoted sulfated zirconia: 2.0FeSZ-1 (squares) and 2.0FeSZ-2-L (stars). **b)** 0.5 wt% Mn-promoted sulfated zirconia: 0.5MnSZ-1 (squares).

batch size. Samples promoted with 2 wt% Fe or Mn showed comparable isotherm shapes for the same calcination batch sizes. The isotherms of the samples with low Mn content, 0.5MnSZ-1-M and 0.5MnSZ-1-L, were characterized by very distinctive H2-loops. Analysis of the adsorption branches of the various catalysts with the BJH method gave unimodal pore size distributions with maximum pore volume at 2.2–3.8 nm and FHWMs of 1–2 nm.

4. Discussion

Events during thermal treatment

An influence of the batch size on the calcination can be envisioned in two ways, namely (i) mass transfer limitations of gas phase species into or out of the powder bed, and (ii) heat transfer limitations. The differences between the samples calcined in differently sized batches are proof of the relevance of such limitations in the calcination chemistry. During the calcination, hydroxide is converted into crystalline zirconium oxide. Norman et al. [36] divided this transformation into three stages, which we converted into a graphical representation (Scheme 1):

1.) Dehydration and loss of terminal hydroxyl groups,
2.) Oxolation of OH bridges and formation of oxide nuclei,
3.) Growth of the nuclei.

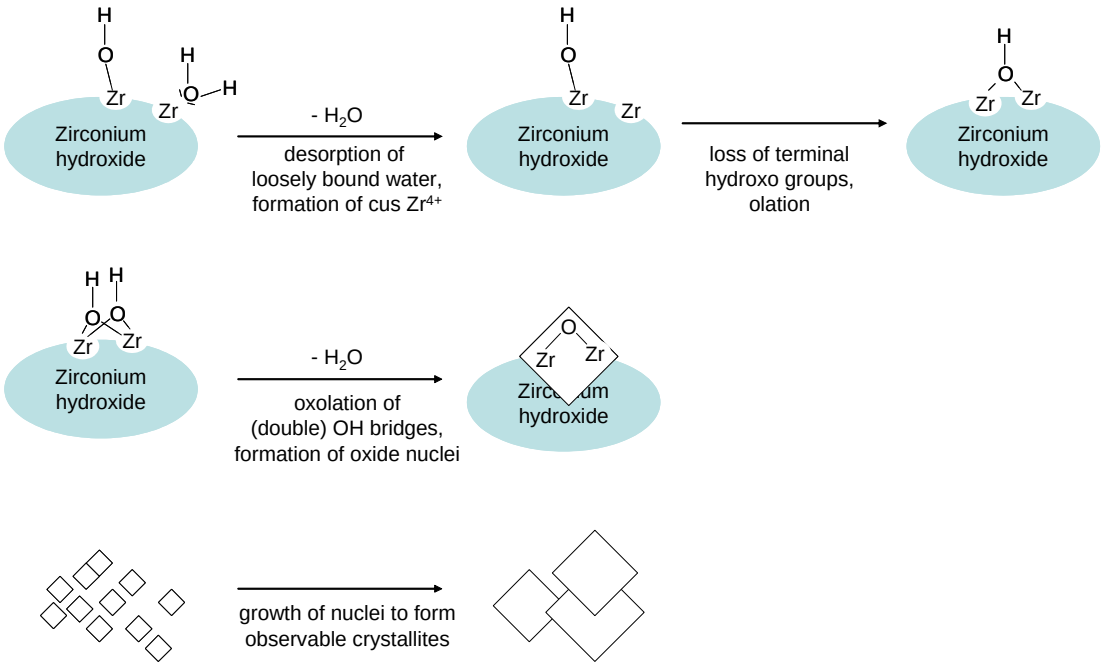

Scheme 1: Crystallization of zirconia from zirconium hydroxide according to description in reference [36].

In the first two steps, heat and mass transfer can already play a role because the produced water needs to be evaporated (endothermic) and transported through the bed. The sample temperature curves (Fig. 1a) indicate a more prominent temperature lag in the larger batches, and water is evaporated more slowly. Retention of water vapor in the tightly packed bed in the larger batches may, via local equilibrium limitation, not only delay dehydration but also dehydroxylation. Norman [36] proposed that at high water vapor pressure, water loss through oxolation would be unfavorable and fewer oxide nuclei would be formed. According to Murase and Kato [37], water vapor increases surface diffusion and markedly accelerates crystallite growth. MS data show most of the water evaporates early and should affect nucleation but not growth. We find a higher surface area with increasing batch size (Table 1), consistent with finer particles. Hence, there was no retention of water vapor in the larger batches and no promotion of crystallite growth through humidity.

The different glow onset temperatures (Fig. 1b) may imply that, already at this stage of the calcination procedure, the materials in differently sized batches are no longer identical and must have undergone e.g. oxolation reactions of different extent. However, the glow event is probably governed by heat transfer limitations. The glow curves indicate explosion kinetics; heat cannot be dissipated as fast as it is produced. This reaction runaway occurs at lower temperature in the large quartz boat with its restricted heat transfer due small surface-to-volume ratio and more complete enclosure of the bed [33].

Norman et al. [36] thought that the three above-listed stages overlap, particularly because they observed a continuous mass loss in thermogravimetry experiments. Chadwick et al. [38] pointed out that dehydroxylation is not complete before crystallization. Djuricic et al. [39] report formation of the tetragonal phase at 573 K without distinct exotherm (separate thermal analysis and XRD experiments). A sharp exotherm at 683–693 K was not accompanied by any sudden change of lattice parameters and was attributed to loss of internal surface hydroxyl groups. Srinivasan and Davis [31] support the idea of separate events and suggest the exotherm to be a result of coalescence of small particles to larger ones, which, for pure zirconium hydroxide, happens to coincide with crystallization. Sorrentino et al. [29] studied a number of other oxides and concluded that coalescence of particles is responsible for the glow. On the other hand Keshavaraja et al. [27] and Livage et al. [40] associate the glow exotherm with crystallization. In summary, the literature does not clearly identify the reaction providing the heat for the glow.

To estimate which of the reactions may produce the measured temperature overshoot, heats of reaction and the specific heat capacity (of the material at the glow onset) need to be known. The glow occurs so rapidly that quasi-adiabatic conditions can be assumed. The heat evolution from surface area loss can be derived from calculated surface energies [41], which approximate the surface enthalpy [42]. For t-ZrO_2, values between 1.107 and 1.453 $J \cdot m^{-2}$ are reported for different surfaces. A loss of 122 $m^2 \cdot g^{-1}$ as found in the zirconia sample would produce 16.5–21.8 $kJ \cdot mol^{-1}$. Values reported for the specific heat capacity range from 0.4 to 0.67 $J \cdot g^{-1} \cdot K^{-1}$ depending on composition and temperature [43-46] . Based on these data, the loss of 122 $m^2 \cdot g^{-1}$ surface area would result in a temperature rise of 200–443 K, which compares well to the observed overshoots. As for measured heats of reaction, neither the initial nor the final state is usually exactly defined in a thermodynamic sense with known composition, fraction of crystalline material, and particle or crystallite size. Molodetsky et al. [47] have tried to distinguish surface area from crystallization effects. They report an increase in surface energy for the transition from amorphous to tetragonal zirconia, specifically 14.6 $kJ \cdot mol^{-1}$ for a material with 100 $m^2 \cdot g^{-1}$ surface area, and an enthalpy of crystallization of tetragonal zirconia of -53 $kJ \cdot mol^{-1}$. According to these and other data [27,40] crystallization also generates enough heat to explain the dramatic temperature overshoot.

We found that the calcination atmosphere does not affect the extent of the glow and shifts the onset temperature only marginally (Fig. 1c). Also, no hydrocarbon oxidation products were detected by MS during the glow so that combustion of contaminants can be ruled out as a source of heat.

The diffractogram of a zirconium hydroxide sample subjected to the heating program until just before the glow (Fig. 2a) reveals reflections of the tetragonal and the monoclinic phase. Partial crystallization appears to occur before the glow, consistent with the observations by Djuricic et al. [39]. The crystallization of zirconia progresses further during the glow as diffractograms recorded after the temperature overshoot (Fig. 2a) demonstrate. The BET surface area drops by 122 $m^2 g^{-1}$ during the glow and pores appear. Hence, for pure zirconium hydroxide the crystallization extends over some time (temperature) while surface area loss and pore formation appear linked to the glow event. The in situ XRD experiment with 2 wt% Fe-promoted sulfated zirconium hydroxide confirms that also for promoted materials crystallization starts before the glow. The crystallization process as reflected in the diffractogram is finished to 90% at 810 K. It can be seen in Fig. 1b that at this bed temperature the glow in the small or medium batch has not yet started. During a controlled and slow heat-up (3 $K \cdot min^{-1}$), there is a substantial degree of crystallization before the glow, and this reaction can in principle supply enough heat to afford the observed overshoot. Crystallization thus initiates a series of events, but the main process during the glow is surface area loss. The sequence of events is summarized in Scheme 2.

The question arises whether sample properties are determined by the events during the heat-up phase including the glow or by what is usually reported, and assumed to be the core of the calcination program, i.e. the holding period at high temperature. Chadwick et al. [38] found that zirconia crystallization and crystallite growth do not progress further after 2 h at 773 K or higher temperatures, and Rush et al. [48] showed that oxygen in amorphous sur

Scheme 2: Course of events during calcination. Temperature ranges approximate and depending on sample and heating conditions. Events may also overlap.

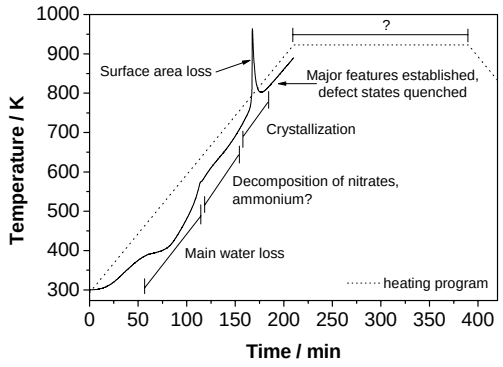

roundings and hydroxyls disappear upon calcination at temperatures from 773 K to 973 K. These observations suggest that in order to determine the final state, the reaching of a certain temperature and a certain holding time are essential. Our data reveal a different picture. The nitrogen adsorption measurement and diffractogram of the zirconia sample that was cooled down directly after the glow largely correspond to those of zirconia samples that underwent the complete heating program. Phase composition and surface area are already established directly after the glow. The subsequent three hour long thermal treatment at 823 K (923 K) does not equalize differences that develop in the early phase of the calcination procedure. During the glow, the maximum programmed temperature is exceeded, which allows for a chemistry that is not possible within the planned temperature program. This includes enhanced ion mobility within the forming solid but also volatilization and re-anchoring with restructuring of surface species. Through the fairly rapid cool-down after the glow non-equilibrium states such as defects in the bulk are quenched. The holding temperature is obviously not high enough to afford annealing of defects generated during the glow. It follows that important sample characteristics, including activity, depend on the extrinsic parameters that rule the events during the heat-up phase such as bed size and packing.

Effect of promoters on sample temperature curve during calcination

The temperature lag caused by the endothermic evaporation of water is less pronounced with increasing promoter content (Fig. 1a); altered by the incipient wetness process, the surface releases less water. In part, the evolving water must have been adsorbed, but it also originates from oxolation (step 2 above, see also Scheme 1). Nitrate or promoter cations may have substituted OH groups or protons on the surface and oxolation will be hindered because water can no longer be cleaved out. Olation and oxolation reactions can also occur between groups located on different particles and can be seen as a pre-stage to coalescence, and the suppression of these reactions explains the higher surface area of the promoted samples. The promoters thus have an influence on the zirconium hydroxide matrix transformation during an early stage of the calcination program. The addition of promoters also influences the redox chemistry during calcination. Nitrate is available as an oxidant. The ratio of nitrate to ammonium varies with the promoter content. The ratio also differs for the promoters Mn and Fe due to the initial valences Mn(II) and Fe(III) and can in principle account for differences between the correspondingly promoted catalysts.

As shown previously, any additive will shift the glow onset to higher temperatures; besides for sulfate [33,49], Mn [27,33], and Fe [33,50] this effect has been reported for hafnium [31] and yttrium [51]. In our sulfated samples, Mn exerts a stronger effect than Fe. No local accumulation of Mn is found by SEM-EDX in the calcined samples. The 10 K step in sample temperature before the glow (Figs. 1b, 1d), which may be caused by a fraction of material with lower promoter content, appears for Fe- but not Mn-promotion. These observations suggest a better dispersion of Mn in comparison to Fe, possibly because of stronger interaction with the hydroxide matrix. Consistently, a higher fraction of Mn than Fe is present in the form of a solid solution in zirconia in the calcined material [23].

Morphology of calcined materials

For Fe-promoted samples, there seems to be a correlation between Fe distribution and morphology. Analysis with SEM-EDX reveals higher Fe concentrations on rough surfaces. Such an elemental distribution could be a consequence of the incipient wetness method. A rough appearance may indicate small particles with a high surface area, and a droplet of impregnation solution may be completely absorbed in the (rough) outer layer. Mn is evenly distributed, indicating a higher mobility of Mn cations in the matrix during the impregnation and calcination procedures. As discussed before, high promoter surface concentrations may hinder the coalescence of particles, which explains the higher surface areas of Fe-promoted in comparison to Mn-promoted samples.

Variation of the calcination batch size affects the morphology. Aggregates of smooth spherical subunits were most obvious for Mn-promoted samples calcined in small batches. These samples experience the longest heat-up period before the glow, leaving time for particles to coalesce and resulting in the smallest surface areas of all promoted samples (Table 1). The porosity varies strongly depending on the calcination batch size. The samples from the large batches are characterized by a system of interconnected mesopores, which lead to the pronounced hysteresis loops in the nitrogen adsorption isotherms. The size of these pores is 2.2–3.8 nm, which is large relative to the kinetic diameter of *n*-butane (0.43 nm). However, since according to the manufacturer, the zirconium hydroxide precursor is microporous [52], the question arises as to

whether micropores are also present in the calcined samples. It was recently reported that neither the isotherm shape nor the de Boer t-plot alone gives reliable evidence for micropores [53]. Further specifics of our data are not in favor of microporosity. First, adsorption and desorption branches coincide perfectly for small values of p/p_0 in all measurements. BET-plots were strictly linear up to p/p_0 = 0.2, and the c values (54–76, Table 1) were in the range typical of non-microporous solids. The BJH adsorption cumulative pore area agreed with the BET surface area within 20%, a deviation that is considered normal [54]. The fact that samples calcined in small batches systematically showed larger BET than BJH surfaces is a possible indication of microporosity but it can be explained by limitations of the oversimplified BJH model, which assumes cylindrical pores. For all sets of isotherms, the evolution of the H2 hysteresis and therefore the change of pore shape coincide with the jump in the BJH cumulative pore area (Fig. 5, Table 1). On the basis of this concurrent behavior, significant amounts of micropores can be excluded.

Isomerization activity

The activity of samples calcined using the same batch size differs much less than those of samples calcined in differently sized batches (Figs. 3a and 3b), the same is true for the characterization data (Table 1 and Fig. 5a). Variations in activity that we still observe for samples calcined using the same batch size are much smaller than those reported for repeated preparations in the literature [24] even though we compared samples from different precursor batches, i.e. the remaining variations will in part be due to the manually conducted impregnation. Hence, attention to the calcination batch size and shape allows the reproducible synthesis of sulfated zirconia catalysts.

It has been inferred that a certain calcination temperature is necessary to generate active sulfate species. For unpromoted sulfated zirconia, the isomerization activity increases with the calcination temperatures until about 923 K, then sulfur loss, surface area reduction and phase transformation lead to a decrease in activity [2,25,55]. The flash-like rise to high temperatures during the glow may generate active sulfur species without the negative side effects. Sulfur species may not be volatilized during the brief overheating or may be re-adsorbed upon cool-down, particularly in the larger and thus deeper beds. No sulfur is detected in the effluent gases during the entire calcination. The restricted time at high temperature also limits particle growth and annealing.

Within each sample set of three, maximum conversion, BET surface area and pore volume increase with increasing calcination batch size. When comparing samples from different sets at equal batch size the maximum conversions also follow the trend of the surface areas. In other words, independent of promoter type or content, the conversions reflect the trends in surface area and porosity. However, the maximum butane conversion increases more than linearly with the corresponding BET surface areas as can be seen from Fig. 6. This becomes more obvious when considering that towards smaller surface areas (< 85 $m^2 \cdot g^{-1}$), the activity will probably not approach zero.

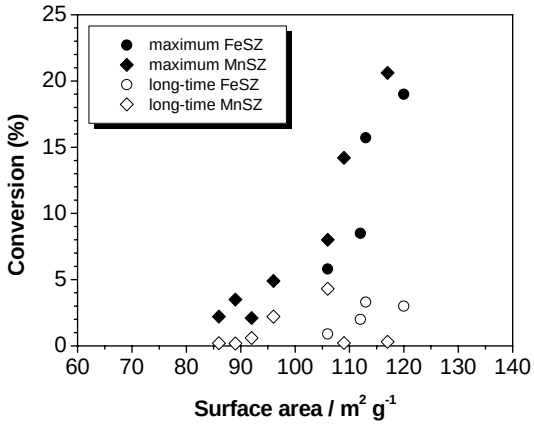

Figure 6: Conversion versus BET surface areas for Fe-promoted (circles) and Mn-promoted (diamonds) sulfated zirconia. Conversion data see Fig. 3; surface areas see Table 1.

The long-term activity is more difficult to evaluate because we do not yet know if and how it is affected by the events at early times on stream; e.g. high conversions may favor deactivation. However, all of the three considered sets deactivate in a different manner but with the same outcome: there is no proportionality between the long-term butane isomerization rate and BET surface areas (Fig. 6) or porosity. This is most obvious when relating the isotherms of 0.5MnSZ-1 (Fig. 5b), which deactivates very little, with the respective conversion data (Fig. 3c). The largest difference in surface area and porosity is between the samples from small and medium batch calcinations, but there is no comparable step in the long-term activity.

There is no simple linear correlation between conversion and surface area, neither for short nor for long times on stream. The number of active sites on these catalysts is small [56] and only a fraction of the sulfate is active. The site concentration thus does not have to scale with the surface area and also depends on structural and chemical properties. Time-on-stream profiles are a function of promoter type and content and not of the calcination batch size, indicating that variation of the batch size affects mainly the number but not the nature of sites.

The redox chemistry during the thermal treatment may also play a role, and it will be more complex if the raw material is promoted. The exothermic formation of N_2 can be ascribed to comproportionation of ammonium and nitrate from the sulfate and promoter precursors. The ratio of ammonium and nitrate varies with the promoter content, and hence the net oxidizing or reducing power. We have evidence that redox reactions during thermal treatment affect the catalytic performance: Fe-promoted catalysts experience very similar glow curves (Fig. 1c) in different

atmospheres but the short- and long-term activities decrease in the sequence oxygen > air > argon (Fig. 3d). It is evident that samples with truly identical thermal history need not be identical. Heat treatment conditions that produce a suitable temperature profile are only a necessary but not a sufficient requirement for good isomerization performance. We do not yet know what the key effect of the variation in oxygen partial pressure might be; obviously Fe, S or Zr valences could be affected. Reduced surface species would diminish the ability of the catalyst to initiate the reaction via oxidative dehydrogenation, which is one of the proposed mechanisms [18]. On the other hand, partially reduced cations in the zirconia bulk, Zr and also Fe, which is known to be incorporated into the zirconia lattice [23] would increase the number of oxygen vacancies in the zirconia lattice. Anion vacancies in sulfated zirconia [57] and promoted sulfated zirconia [23] have been suspected to assist in the *n*-butane isomerization.

Comparison of the rate data with published data is only possible for 323 K and under the assumption of a 1st order reaction in *n*-butane. The maximum isomerization rates obtained for the samples calcined in large batches at 323 K (not shown) are 400 (Mn) – 435 (Fe) $\mu mol \cdot g^{-1} \cdot h^{-1}$ at 1 kPa *n*-butane; reported rates reach 1800 $\mu mol \cdot g^{-1} \cdot h^{-1}$ (mixed Fe + Mn promotion) at 10 kPa *n*-butane [58]. Hence, with respect to the maximum rate, extraordinarily active catalysts can be obtained via calcination in large batches.

5. Conclusions

The properties of sulfated zirconia catalysts become reproducible through controlling the batch size and shape during calcination. These parameters as well as temperature, holding time, heating rates, and gas flows should be reported. In turn, without altering the precursor composition or the heating program for calcination, the morphological and catalytic properties of sulfated zirconia materials can be tuned through variation of the batch size. Samples sets obtained in this manner provide a unique opportunity to identify structure-activity relationships because many preparation parameters are identical and accordingly, many properties will be identical and can then be considered irrelevant for differences in activity.

The maximum *n*-butane isomerization rate of Fe- or Mn-promoted sulfated zirconia catalysts increases with the batch size used for calcination. This trend is paralleled by an increase in surface areas and a growing system of interconnected mesopores. The long-term activity, which also increases with batch size unless there is complete deactivation, seems unrelated to surface area or porosity. Hence, the concentration of the active sites must depend on structural and chemical properties. The observed influence of the batch size implies these sites must develop during the glow, i.e. the active phase is formed rapidly. Promoter concentration and type affect this chemistry. The fact that differences generated in the heating period are not annulled during the subsequent 3 h treatment at 823 or 923 K suggests that non-equilibrium structures such as defects in the lattice, which are generated by kinetic and not by thermodynamic control, must constitute the active phase of these catalysts.

Normalized to surface area, Mn-promoted catalysts are slightly more active than Fe-promoted catalysts (Fig. 6), suggesting they have a higher site concentration or sites of higher activity. The more complete incorporation of Mn into the zirconia lattice in comparison to iron [23], the glow curves and the chemical analysis all demonstrate that Mn is more highly dispersed than Fe. Low concentrations of Mn are already very effective. These observations indicate that Mn or Fe ions distributed on the surface or in the lattice, and not a promoter oxide phase, are the cause of the promotional effect.

6. Acknowledgement

The authors wish to thank Rachel Caruso for her kindness and help during the nitrogen adsorption measurements at the Max Planck Institute for Colloid and Interface Science at Golm. Gisela Lorenz is acknowledged for sample preparation and Edith Kitzelmann for performing X-ray diffraction measurements.

References

1. M. Hino, S. Kobayashi, K. Arata, J. Am. Chem. Soc. 101 (1979) 6439.
2. X. Song, Y. Sayari, Catal. Rev.-Sci. Eng. 38 (1996) 329.
3. T.-K. Cheung, J.L. d'Itri, B.C. Gates, J. Catal. 151 (1995) 464.
4. T.-K. Cheung, F.C. Lange, B.C. Gates, J. Catal. 159 (1996) 99.
5. M. Hino, K. Arata, J. Chem. Soc., Chem. Commun. (1980) 851.
6. V. Adeeva, J.W. de Haan, J. Jänchen, G.D. Lei, V. Schünemann, L.J.M. van de Ven, W.M.H. Sachtler, R.A. van Santen, J. Catal. 151 (1995) 364.
7. L.M. Kustov, V.B. Kazansky, F. Figueras, D. Tichit, J. Catal. 150 (1994) 143.
8. C. Morterra, G. Cerrato, F. Pinna, M. Signoretto, J. Catal. 157 (1995) 109.
9. W. Stichert, F. Schüth, J. Catal. 174 (1998) 242.
10. X. Yang, F.C. Jentoft, R.E. Jentoft, F. Girgsdies, T. Ressler, Catal. Lett. 81 (2002) 25.
11. C.-Y. Hsu, C.R. Heimbuch, C.T. Armes, B.C. Gates, J. Chem. Soc., Chem. Commun. (1992) 1645.
12. F.C. Lange, T.-K. Cheung, B.C. Gates, Catal. Lett. 41 (1996) 95.
13. M.A. Coelho, D.E. Resasco, E.C. Sikabwe, R.L. White, Catal. Lett. 32 (1995) 253.
14. C.-H. Lin, C.-Y. Hsu, J. Chem. Soc., Chem. Commun. (1992) 1479.
15. A. Jatia, C. Chang, J.D. MacLeod, T. Okubo, M.E. Davis, Catal. Lett. 25 (1994) 21-28.
16. R. Srinivasan, R.A. Keogh, A. Ghenciu, D. Fărcaşiu, B.H. Davis, J. Catal. 158 (1996) 502.
17. E.C. Sikabwe, M.A. Coelho, D.E. Resasco, R.L. White, Catal. Lett. 34 (1995) 23-30.

18. K.T. Wan, C.B. Khouw, M.E. Davis, J. Catal. 158 (1996) 311.
19. T. Yamamoto, T. Tanaka, S. Takenaka, S. Yoshida, T. Onari, Y. Takahashi, T. Kosaka, S. Hasegawa, M. Kudo, J. Phys. Chem. B 103 (1999) 2385.
20. R.E. Jentoft, A. Hahn, F.C. Jentoft, T. Ressler, Physica Scripta T115 (2005) 794.
21. R.E. Jentoft, A.H.P. Hahn, F.C. Jentoft, T. Ressler, Phys. Chem. Chem. Phys. 7 (2005) 2830.
22. J.M. Millet, M. Signoretto, P. Bonville, Catal. Lett. 64 (2000) 135.
23. F.C. Jentoft, A. Hahn, J. Kröhnert, G. Lorenz, R.E. Jentoft, T. Ressler, U. Wild, R. Schlögl, J. Catal. 224 (2004) 124.
24. R.A. Keogh, R. Srinivasan, B.H. Davis, J. Catal. 151 (1995) 292.
25. F.R. Chen, G. Coudurier, J.-F. Joly, J.C. Védrine, J. Catal. 143 (1993) 616.
26. S.X. Song, R.A. Kydd, Catal. Lett. 51 (1998) 95.
27. A.Keshavaraja, N.E. Jacob, A.V. Ramaswamy, Thermochim. Acta 254 (1995) 267.
28. L. Wöhler, Koll.-Zeitschr. 38 (1926) 97.
29. M. Sorrentino, L. Steinbrecher, F. Hazel, J. Colloid Interface Sci. 31 (1969) 307.
30. J.D. Carruthers, K.S.W. Sing, J. Feenerty, Nature 213 (1967) 66.
31. R. Srinivasan, B. H. Davis, J. Colloid Interface Sci. 156 (1993) 400.
32. T. Tatsumi, H. Matsuhashi, K. Arata, Bull. Chem. Soc. Jpn. 69 (1996) 1191.
33. A. Hahn, T. Ressler, R.E. Jentoft, F.C. Jentoft, J. Chem. Soc., Chem. Commun. (2001) 537, electronic support information: http://www.rsc.org/suppdata/CC/b1/b100364j/index.sht.
34. B.S. Klose, R.E. Jentoft, A. Hahn, T. Ressler, J. Kröhnert, S. Wrabetz, X. Yang, F.C. Jentoft, J. Catal. 217 (2003) 487.
35. K.S.W. Sing, D.H. Everett, R.A.W. Haul, L. Moscou, R.A. Pierotti, J. Rouquérol, T. Siemieniewska, Pure Appl. Chem. 57 (1985) 603.
36. C.J. Norman, P.A. Goulding, I. McAlpine, Catal. Today 20 (1994) 313.
37. Y. Murase, E. Kato, J. Am. Ceram. Soc. 66 (1983) 196.
38. A.V. Chadwick, G. Mountjoy, V.M. Nield, I.J.F. Poplett, M.E. Smith, J.H. Strange, M.G. Tucker, Chem. Mater. 13 (2001) 1219.
39. B. Djuricic, S. Pickering, D. McGarry, P. Glaude, P. Tambuyser, K. Schuster, Ceram. Int. 21 (1995) 195.
40. J. Livage, K. Doi, C. Mazières, J. Am. Ceram. Soc. 51 (1968) 349.
41. A. Hofmann, S.J. Clark, M. Oppel, I. Hahndorf, Phys. Chem. Chem. Phys. 4 (2002) 3500.
42. A.W. Adamson, Physical Chemistry of Surfaces, Wiley, New York, 1990, p. 54.
43. R. Ruer, Z. Anorg. Allg. Chem. 43 (1905) 282.
44. Manufacturer information, Dynamic-Ceramic Ltd., Crewe, UK.
45. H. Moore, J. Soc. Glass Technol. 23 (1939) 371.
46. T. Tojo, T. Atake, T. Shirakami, T. Mori, H. Yamamura, Solid State Ionics 86-88 (1996) 89.
47. A. Molodetsky, A. Navrotsky, M.J. Paskowitz, V.J. Leppert, S.H. Risbud, J. Non-Cryst. Solids 262 (2000) 106.
48. G.E. Rush, A.V. Chadwick, I. Kosacki, H.U. Anderson, J. Phys. Chem. B 104 (2000) 9597.
49. S. Chokkaram, R. Srinivasan, D.R. Milburn, B.H. Davis, J. Colloid Interface Sci. 165 (1994) 160.
50. R. Srinivasan, R.A. Keogh, B.H. Davis, Appl. Catal. A: General 130 (1995) 135.
51. K. Haberko, A. Ciesla, A. Pron, Ceramurgia International 1,3 (1975) 111.
52. MELCat Doc 6140, MEL Chemicals, Manchester, UK.
53. S. Storck, H. Bretinger, W.F. Maier, Appl. Catal. A: General 174 (1998) 137.
54. S.J. Gregg, K.S.W. Sing, Adsorption, Surface Area and Porosity, 2nd ed., Academic Press, London, 1982.
55. D. Fraenkel, Ind. Eng. Chem. Res. 36 (1997) 52.
56. S.Y. Kim, J.G. Goodwin Jr., D. Galloway, Catal. Today 63 (2000) 21-32.
57. C.R. Vera, C.L. Pieck, K. Shimizu, J.M. Parera, Appl. Catal. 230 (2002) 137.
58. A. Sayari, Y. Yang, J. Catal. 187 (1999) 186